Assessment of the Efficiency of Prefabricated Hybrid Composite Plates (HCPs) for Retrofitting of Damaged Interior RC Beam-Column Joints

Esmaeel Esmaeeli[a], Joaquim A. O. Barros[b], Jose Sena-Cruz[c], Humberto Varum[d], José Melo[e]

[a] PhD Candidate, ISISE, Dept. Civil Eng., University of Minho, Guimarães, Portugal, esmaeeli_civil@outlook.com

[b] Full Professor, ISISE, Dept. Civil Eng., University of Minho, Guimarães, Portugal, barros@civil.uminho.pt

[c] Associate Professor, ISISE, Dept. Civil Eng., University of Minho, Guimarães, Portugal, jsena@civil.uminho.pt

[d] Associate Professor, Dept. Civil Eng., University of Aveiro, Portugal, hvarum@ua.pt

[e] PhD Candidate, Dept. Civil Eng., University of Aveiro, Portugal, josemelo@ua.pt

Corresponding Author Contacts:

Esmaeel Esmaeeli

ISISE, Dep. Civil Eng., School Eng., University of Minho

Campus de Azurém,

4800-058 Guimarães, Portugal

Tel: +351 917 40 90 75

Email: esmaeeli_civil@outlook.com

Abstract

The effectiveness of prefabricated hybrid composite plates (HCPs) as a seismic retrofitting solution for damaged interior RC beam-column joints is experimentally studied. HCP is composed of a thin plate made of strain hardening cementitious composite (SHCC) reinforced with CFRP sheets/laminates. Two full-scale severely damaged interior beam-column joints are retrofitted using two different configurations of HCPs. The effectiveness of these retrofitting solutions mainly in terms of hysteretic response, dissipated energy, degradation of secant stiffness, displacement ductility and failure modes are compared to their virgin states. According to these criteria, both solutions resulted in superior responses regarding the ones registered in their virgin states.

Keywords: Strain Hardening Cementitious Composite (SHCC); Carbon Fibre Reinforced Polymer (CFRP); Hybrid Composite Plate (HCP); Interior Reinforced Concrete (RC) beam-column joint; Cyclic behaviour; Retrofitting.

1. Introduction

The performance of each element composing framed systems in reinforced concrete (RC) structures has direct impact on their global response to withstand lateral seismic demands. High inelastic rotation capacity of the beams at the vicinity of the connection to the column, sufficient shear strength and stiffness of the beam-column joint panels, and a predominant elastic response of the columns will allow the dissipation of a high amount of the energy, if the stability of the structure to transfer the gravity load to its supports is assured. According to the provisions of the modern codes oriented to seismic design, the capacity hierarchy design, along with a proper detailing of the internal steel arrangement should be taken into account to achieve such a ductile and safe response of the designed RC structures located in moderate and high seismic risk zones. However, there are a considerable number of existing RC structures designed with previous codes, with only Gravity Load Design (GLD) approaches, especially those designed according to pre-1970th codes provisions. These structures have, in general, inadequate detailing to resist the lateral demands induced by earthquake actions. Recognizing these deficiencies, the scientific community working on structural seismic design and retrofitting started proposing several strategies for the seismic rehabilitation and retrofitting [1, 2]. Steel jacketing, cast-in-place concrete/RC jacketing [3], shotcrete jacketing [4], epoxy injection repair [5], application of Fibre Reinforced Polymers (FRPs) [3, 5-13] are the proposed solutions that can be found in literature as common strengthening/repair solutions. Among the aforementioned techniques, FRP materials have attracted special attention of several researchers, mainly due to their lightweight, flexibility for practical application and easiness of application. These composite materials are used in the shape of externally bonded sheets or laminates. The main practical challenge for using FRP in the retrofitting of RC elements is related to their premature de-bonding [14]. In general, mechanical anchors are proposed in an attempt of preventing/delaying debonding, or even to assure the ultimate capacity of the composite material. The research carried out by Engindeniz et al. [15] on the retrofitting of both damaged and undamaged three-dimensional beam-column-slab joint specimens clearly highlighted the important role of proper anchoring for the FRP systems, since debonding was the main failure mechanism, avoiding the full exploitation of the strengthening potentialities of these materials. However, special attention is needed to prevent high stress concentrations around the anchored zone in order to avoid premature rupture of FRP. Anchoring FRP material bonded to the top and bottom faces of a beam inside a groove, executed at the concrete cover of the column, is proposed as an alternative solution to transfer tensile stresses of the FRP material behind the critical section at beam-column interface [7, 16]. However, this

technique is limited to the depth of concrete cover and might involve the risk of introducing damage to the column's longitudinal bars during the carving of the groove. Moreover, the joint region should resist higher demands associated to the shear stresses introduced by FRP anchorage while shear deficiency of this zone is one the most common vulnerabilities known in RC structures with seismic retrofitting requirements. The solution studied by Mukherjee and Joshi [7] based on using the "L" shape FRP strengthening technique in combination with FRP wraps on both beam and column elements might be an alternative to partially treat the aforementioned concerns. Besides the aforementioned practical drawback, the properties of FRP materials are negatively affected by temperatures higher than the glass transition temperature of the adhesive used in these materials and in FRP-based strengthening techniques (epoxy is the most used adhesive). Moreover, the composite layer needs to be protected against vandalism. A comprehensive review on FRP durability issues is reported by Benmokrane and Mohamed [17].

Strain hardening cementitious composite (SHCC) is a class of Fibre Reinforced Concretes (FRCs), with the character of developing a continuous increase of post-cracking tensile capacity up to the stress localization at one of the multiple formed cracks for a relatively high tensile strain. The formation of multiple diffused hairline cracks through all the loaded length of the specimen during the hardening stage assures levels of ductility not possible to attain in conventional FRCs. By testing in bending masonry elements strengthened with a thin layer of SHCC applied to their bottom face, Esmaeeli et al. [18] demonstrated that higher load carrying capacity and ductility is achievable when compared to flexural strengthening methodologies based on the use of thicker layers of ordinary steel FRC.

Recently Esmaeeli et al. [19] have investigated the effectiveness of a new technique for the shear strengthening of short-span shear deficient beams. The strengthening element, nominated as Hybrid Composite Plate (HCP), combines the potential structural effectiveness of prefabricated plates made of SHCC with carbon fibre reinforced polymer (CFRP) sheets for the shear strengthening of deep beams. In fact, covering the internal surface of the SHCC plate with a CFRP sheet results in mutual advantages for these materials: in the durability perspective the SHCC provides protection for the CFRP, adding an extra safety against the detrimental effects of vandalism, and cycles of relatively high humidity and temperature; in its turn the CFRP increases significantly the tensile capacity for the HCP. Furthermore, the SHCC contributes to increase the resistance of the compressive strut, and to restrain the propagation of macro cracks due to the fibre reinforcing mechanisms, being expectable much higher load carrying capacity and deformation performance.

In the present study the effectiveness of HCP to retrofit full-scale damaged GLD interior beam-column joints is investigated. HCPs are attached to the damaged interior beam-column joints by means of epoxy resin and chemical anchors to partially cover these framed elements. Two different configurations of HCPs were used: (i) a cross shape SHCC plate reinforced with CFRP laminates according to the near surface mounting (NSM) technique [20]; (ii) SHCC plates reinforced with externally bonded CFRP sheets forming an "L" shape configuration.

2. Experimental Program

The experimental program comprised the retrofitting of two full-scale damaged interior beam-column joints. After retrofitting, these specimens were subjected to the same loading history as previously imposed in their virgin state. To assess the effectiveness of each of the two proposed HCP-based retrofitting solutions, the results determined in the strengthened specimens are compared to those obtained in the corresponding specimens in the virgin state. The performance of both strengthening strategies is also compared.

2.1. Damaged Specimens

Two damaged interior RC beam-column joints were selected among a series of tested specimens. These specimens were the subject of an experimental research in the scope of a PhD thesis [21, 22]. Configurations of pre-1970th RC buildings were adopted for the design process of these framed elements. Therefore, plain steel bars were used as the reinforcement of beams and columns of these specimens. No transverse reinforcement in the joint region was applied, and 90° hook arrangement was adopted for the stirrups and hoops in beams and columns, respectively. The beams and the columns of these full-scale specimens had a length of the half-span and the half-story, respectively, of common RC buildings. This configuration of the elements allows representing the behaviour of the beam-column joint assemblage under lateral loading, considering the end-points in beams and columns of the specimens where the moment inflection is expected to occur. The geometries and steel configurations of the selected specimens for the retrofit, JPA0 and JPC, are shown in Figure 1. It should be noted that the shorter length adopted for the inferior column of the specimens, associated to a steel element with equivalent stiffness, allows to represent the behaviour of the assemblage and to accommodate the load cells and pin connection at the bottom of the column, as it is evident in the test setup.

The average concrete compressive strength, measured in cubes of 150 mm edge, was equal to 23.8 MPa with an estimated characteristic compressive strength of 19.8 MPa, corresponding to the C16/C20 concrete strength class

according to the grades existing in EC2-1992-1-1 [23]. By performing tensile tests on steel bars, average values of 590 MPa and 640 MPa were determined for the yield and the ultimate tensile strength of the longitudinal reinforcement, respectively, with an elasticity modulus of 198 GPa.

A lateral reversal displacement history was imposed to the top of the superior column combined with a constant axial load of 450 kN. This axial force represents the gravity load corresponding to an axial compressive stress of 21.3% of the average concrete compressive strength. The lateral load was constituted of a series of displacement-controlled cycles, in push (positive displacement) and pull (negative displacement) direction, with an incremental magnitude up to 4% interstory drift. After three cycles of loading that introduced a drift level of 0.13%, each level of displacement was repeated three times, as it is shown in Figure 2. The specimens were tested horizontally according to the test setup illustrated in Figure 3.

The maximum load carrying capacity of 43.2 kN and 38.3 kN was registered for JPA0 and JPC, respectively, at the drift levels of 2.7% and 3.3%.

According to PA damage index proposed by Park and Ang [24], these damaged specimens can be categorized as "collapsed" due to the extensive damage that they experienced during tests [21].

As consequence of deficient bond between smooth longitudinal bars and the surrounding concrete, the damages at the end of the test were mainly localized in the vicinity of the joint region into the beams and columns. As shown in Figure 4, the extent of the damages includes concrete crushing and spalling off at the intersections of the beams and the columns, severe sliding of longitudinal reinforcement due to significant bond deterioration and, eventually, flexural cracks localized at the beam-joint interfaces or column-joint interfaces. In JPA0 one of the flexural cracks was, however, localized at a certain distance from the joint region (Figure 4a). Additional information about experimental program and test results of the virgin specimens can be found elsewhere [21].

2.2. Retrofitting Strategy

The retrofitting schemes for the both damaged specimens were based on attaching cross shape HCPs to the front and rear faces of the beam-column joint. However, for the case of JPC, additional "L" shaped HPCs were also attached to the lateral faces of the beam-column at each corner. The cross shape HCPs have partially covered the overall length of the specimens (Figure 5). The depth of the sections covering the beams was 390 mm, while for the columns was 290 mm. The HCP had an overall thickness of 25 mm, which was sufficient to accommodate two layers of CFRP laminates of cross section of 10 mm×1.4 mm, in two different levels (in orthogonal directions). This

configuration provided a 5 mm protecting cover against the environmental actions for the epoxy used to fix CFRP laminates inside the grooves of the HCP. The grooves were cut with 5 mm of width, and 10 mm or 20 mm of depth, depending on the level that CFRP laminates were supposed to be placed (Figure 5c).

The longitudinal reinforcement of the HCPs included pairs of continuous laminates in the direction of beam's and column's axis (Figure 5a to Figure 5c). Consequently, the laminates located in the beams were placed in a different level than the ones of the columns. In the HCPs used to retrofit JPA0, the spacing of the transverse CFRP laminates was 100 mm (Figure 5a). This distance was maintained in the portions of the HCPs that were covering the columns of the JPC-R specimen, while in the part of HCP applied in the beams of this specimen the spacing of the transverse CFRP laminates was increased to 200 mm in order to take into account the smaller spacing of steel stirrups in the beams (Figure 5b). At the joint region of both series of the HCPs, pair of CFRP laminates forming an "X" shape configuration was mounted in an attempt of increasing the shear resistance of the joint. A combination of the S&P 220 epoxy resin and chemical anchors (Hilti HIT-V 8.8 with 10 mm diameter) was used as the attaching system for the "Cross shape" HCP to the concrete substrate. As it was already mentioned, for the case of JPC, additional HCPs, composed of two SHCC plates reinforced with one layer of externally bonded unidirectional CFRP sheet with an "L" shape configuration, were attached to the faces of the columns and the beams at each corner (Figure 5d). In the case of "L" shape HCPs, S&P 50 epoxy resin and chemical anchors (Hilti HIT-V 8.8 with 10 mm diameter) were used to fix these panels to the lateral faces of beams and columns. To the retrofitted JPC and JPA0 specimens, the nomination of the JPC-R and JPA0-R was attributed, respectively.

All the retrofitting process was performed with the specimens in horizontal position. For both specimens the remaining crushed and spalled off concrete at the corners of the joints was removed and then replaced with Sika Grout-213. To seal the cracks, boreholes were drilled through the cracked sections. After cleaning the holes using compressed air, small diameter pipes were placed inside them, then the superior face of the cracks was sealed and then epoxy resin SikaDur-52 was injected through these pipes. After turning the specimens, the sealing process was repeated to assure that the cracked section was sealed as much as possible. The concrete substrate was also slightly roughened using hand-held concrete scabbler to partially expose the aggregates. This surface roughening aims to improve the HCP-concrete interface bond properties. Prior to the installation of the HCPs, chemical anchors were mounted inside the holes perforated on the beams, columns and joint regions, at the positions represented in Figure 5. Before mounting the anchors, the holes were partially filled with Hilti Hit-HY 200-A as a fast curing injectable

bonding agent. The embedded length of the anchors inside the concrete was 115 mm. Figure 6 shows a view of the specimens after the HCPs have been applied.

2.3. Material Properties of Retrofitting System

The self-compacting SHCC was composed of a cementitious mortar reinforced with 2% of volume short discrete PVA fibres. The PVA fibre used in this study had a length of 8 mm and was produced by Kuraray Company with designation of RECs15×8. The average tensile stress at crack initiation and the average tensile strength of the SHCC was 2.43 MPa and 3.35 MPa, respectively, with a minimum tensile strain capacity of 1.3%. More details on mixture ingredients, mixing process and test setup of the SHCC can be found in [18, 19, 25]. The commercial name of the utilized carbon fabric is S&P C-Sheet 240. According to the supplier, this fabric has a tensile elasticity modulus of 240 GPa and a nominal tensile strength of 3800 MPa. The fabric elongation at rupture is 1.55%. The measured thickness of this fabric was 0.3 mm. Based on technical data, S&P 50 epoxy resin develops a tensile strength of 35.8 MPa and a modulus of elasticity around 2.6 GPa at the age of 14 days. An average tensile strength of 18 MPa and average modulus of elasticity of 6.8 GPa were obtained based on uniaxial tensile tests carried out following the recommendations of ISO 527-2:1996 [26] on six dumbbell-shaped S&P 220 epoxy resin after 7 days of curing. Tensile properties of the used CFRP laminate (S&P laminate CFK 150/2000) with a cross section of 1.4×10 mm^2 were characterized following the procedure proposed in ISO 527-5:2009 [27]. From the tests executed in six coupons, average values of 2689 MPa, 1.6% and 165 GPa were obtained for the tensile strength, strain at CFRP rupture and modulus of elasticity, respectively. The average compressive strength of 38.4 MPa for SikaGrout-213 was obtained by means of compression tests on four cubes of 100 mm edge.

2.4. Test Setup and Loading Pattern

The same test setup, cyclic lateral load history and axial load in the columns used for testing the virgin specimens were adopted for testing the retrofitted ones. Figure 7 shows the schematic configuration of the displacement transducers (DTs) mounted on the specimens to measure the local deformations. Four slices along each beam and each column were considered for this purpose. The axial deformation of each region, along the longitudinal CFRP laminates, was registered using a parallel pair of DTs installed in each slice. By combining diagonal, vertical and horizontal DTs in the joint region, the distortion of the panel of the joint was also evaluated.

3. Results and Discussion

3.1. Hysteretic Response

Figure 8 shows the hysteretic responses of both virgin and retrofitted specimens in terms of lateral load *versus* lateral displacement (and drift), registered at the top of the superior column. Both techniques resulted in successful retrofitting solutions in comparison with the results obtained with the corresponding specimen in the virgin state, since higher load carrying capacity was obtained. The pinching effect observed in the reversal loops of JPC was also slightly improved by using the proposed strengthening technique. The values registered for the maximum lateral load (Fp) and the corresponding drifts (d_p) for specimens in the retrofitted and virgin states are indicated in Table 1. The increase level in terms of lateral peak load after strengthening is also indicated in this table. According to the obtained results, the retrofitting technique provided an increase of 25.5% and 18.2% in terms of maximum lateral load carrying capacity of JPA0 for the negative and the positive displacements, respectively. The corresponding values for JPC-R are even larger, so that an increase of 54.5% and 48.3% was obtained for the negative and positive direction, respectively. A relatively different hysteretic response during the positive and negative loading directions for JPC-R is correlated to an unsymmetrical damage distribution and will be discussed further in this paper.

3.2. Damage Evolution and Failure Modes

JPA0-R: The initiation of the first series of cracks occurred at the cycles corresponding to a drift of 0.33%. These cracks were formed at the inferior face of the left beam and also at the inferior and superior face of the right beam at the vicinity of the first series of the anchors, almost inside slice 2 (see Figure 9 and also Figure 7). Further increase in the displacement demand led to the formation of a crack crossing the section of the right beam, while in the left beam the relevant damage seems to have become restricted to the increase of the crack's width on the beam's inferior face. Although a single crack was formed on the lateral faces of the beams, during their widening up to a drift of 1.3% multiple hairline cracks were formed on the surface of HCP at the vicinity of the locations of these cracks. At cycles corresponding to 1% drift, diagonal cracks started to appear at the beam-column intersections. By further increase in the amplitude of the drift cycles, these inclined cracks started propagating toward the opposite corners forming an X shape crack pattern coinciding with the inclined CFRP laminates positioned in the joint of the HCP (Figure 9). When the drift cycles reached the value of 1.3%, horizontal and vertical cracks started to appear inside the joint region, between the intersections of longitudinal CFRP laminates of the beams and columns. At the

drift of 2.0%, the retrofitted corners at the intersection of beams and columns started to spall off. The widening and propagation of the cracks inside the joint region may have governed the failure mode of the JPA0-R specimen. The visual inspection of the joint panel after the test revealed the bulged faces of the HCPs in the joint region with X shape cracks along with crushing of the old concrete, which was confined inside the HCPs.

JPC-R: the onset of the first crack was at the 2nd cycle of the set of cycles corresponding to 0.2% of drift in negative direction (see Figure 2). This crack was formed at the superior face of the right beam in a distance of 80 mm far from the extremity of HCP (on the non-retrofitted region). During the positive displacement of this drift level, a second crack was also observed out of the retrofitted region, at a distance of 40 mm far from the extreme edge of the HCPs on the superior face of the left beam. At 0.33% of negative drift, the first crack has progressed in terms of length and width. At the same level of drift but in the positive direction, a third crack was formed at the inferior face of the right beam in a distance approximately equal to the crack which was already formed at the superior face of this beam.

During the following cycles, the propagation of the existing crack on the left beam seems to have been restricted by the presence of the HCP, while the existing cracks on the right beam have propagated up to become connected. It should be noted that, since the sliding of the longitudinal bars of both beams was restricted by the adoption of 90° bend extremities for these bars, further increase in displacement demand, up to 1.67% drift, was followed by higher load carrying capacity. This higher load is a consequence of the moment redistribution towards other regions of the beam-column assembly not so damaged.

During both the positive and the negative displacements of the cycles corresponding to 1% drift, further cracks on both the left and right beams adjacent to the beam-column interfaces were formed (Figure 10). The sequence of the cracks occurrence was at: i) inferior face of the left beam; ii) inferior face of the right beam; iii) superior face of the right beam; iv) superior face of the left beam. By increasing the drift up to 1.3%, these cracks on the left beam intersected each other. The crack on the inferior face of the right beam has widened and propagated, while the crack at the superior face in this region has only experienced a small increase in its width. This was due to the action of the previously cracked region of the right beam out of the retrofitted zone, which acted as the governing damage region on the right beam. By repeating the cycles with the same level of the drift, the cracks at the vicinity of the beam-column interfaces progressed into the bonded region of the CFRP sheet on the left side of the superior and inferior column, as well as towards the right side of the inferior column. When the drift cycles corresponding to 1.67% were

imposed, this detachment progress met the first level of anchors positioned in the superior and inferior columns. Further detachment of the CFRP sheet in normal and tangential directions was resisted by the flexural resistance of the SHCC plate and bearing capacity of the anchors, respectively. At a drift cycle of 2.67% the SHCC plate reached its flexural-tensile capacity and failed. At the higher levels of drift, only the width of these cracks has increased without any further crack formation. By the end of the test, to visualize the developed micro-cracks, the surface of the HCPs that was varnished before testing, was sprayed with a penetrating liquid. As a result of this technique, it was visible multiple diffuse micro-cracks inside the joint panel zone with diagonal orientation, fish spinal shape micro-cracks along the longitudinal CFRP laminates on the cross shape HCP, and diffuse micro-cracks in the vicinity of macro-cracks around the anchors in the joint region and in the first slice of both beams (see Figure 10 and also Figure 7).

Failure modes: The flexural capacity of the beams was the governing failure mode of JPC-R, while joint shear failure was the governing failure mode for JPA0-R. This joint shear failure can be attributed to the performance of the "L" shape panels attached to the beam-column corners of the JPC-R. In fact, due to the continuity of the strengthening system at the junction of the beams and columns, where they are subjected to the largest bending moments, the "L" shape panel was submitted to high tensile stresses, mainly due to the contribution of the CFRP sheet. The effectiveness of the bond adhesive and anchors, as well as the flexural capacity of the SHCC plate, have assured a proper medium for the transference of these tensile stresses to the interior of the beam and column (therefore lower shear stress were transferred to the joint region) preventing a progressive detachment of the CFRP sheet. In fact the detachment of the CFRP sheet has only propagated up to the position of the first anchor in the column.

3.3. Flexural Capacity of Beams

When the flexural capacity of the columns and the shear capacity of the beams and columns are adequate, the failure mechanism of the interior beam-column joints depends either on the flexural capacity of the beams subjected to reversal loadings or the shear capacity of the joint panel, as it was the case for JPC-R and JPA0-R, respectively. Equation (1) presents the state of the static equilibrium between the maximum developed moments at the left and the right beams with respect to the lateral force at the top of the column.

$$Vc = \frac{M_R + M_L}{L_c} \tag{1}$$

where Vc is the shear force in the column, M_R and M_L are the internal moment developed at the beam-column interface of the right beam and the left beam, respectively. In Eq. (1), L_C is the length of the column between the positions of lateral load at the superior column and the lateral support at the inferior column. Therefore, any reduction in the flexural capacity of the left or right beams may result in the loss of lateral capacity of the beam-column assembly, unless this reduction could be compensated through the moment redistribution into the other parts of the structure.

The maximum moments (at the mid-section of slice 1 on the left and the right beams) *versus* the drift demands were calculated by considering the force values registered in the load cells and equilibrium conditions, and the obtained results are illustrated in Figure 11. For the signs of the internal moments a criterion identical to the lateral displacements was assumed. Therefore, for a positive drift (Figure 2 or Figure 3) the moments generated in the interfaces of beam-column are considered positive, while they are negative for a negative drift (see the schematic representation in Figure 11).

According to Figure 11a, the maximum bending moments developed in the left and the right beams of JPA0-R, during the negative displacement, were -92.95 kN·m at a drift of -3.00% and -54.03 kN·m at a -2.65% drift, respectively. During the positive displacement, the left and the right beams reached their maximum bending moment, +52.11 kN·m and +90.69 kN·m, at drift levels of +2.31% and +2.99%, respectively.

As depicted in Figure 11b, the values of maximum bending moments for JPC-R in the left and the right beams, during the negative displacement were -114.13 kN·m at a drift level of -2.66 % and -55.58 kN·m at -1.65 % of drift, respectively. The developed maximum bending moment for the positive displacement, in the left and the right beams were +51.09N·m and +106.4 kN·m at drift level of +2.64%, respectively. A sudden reduction observed in bending moment capacity of the right beam during negative loading, at drift cycle of 1.67% (Figure 11b), is associated to a noticeable sliding of longitudinal steel bars at the superior face of that beam. Sliding of these bars has initiated out of the retrofitted region where damage was already extensive, and then progressed along the beam toward its supporting extremity. Due to this process a sudden drop in lateral load carrying capacity of JPC-R was registered at this level of drift (Figure 8b), after which the specimen presented a structural softening behaviour for any further loading in the negative direction.

As mentioned when the damage evolution of JPC-R was discussed, at a drift cycle of 2.67% the SHCC plate installed on the lateral face of the column reached its flexural-tensile capacity, and failed. Failure of this plate

resulted in the loss of the contribution of the CFRP sheet for the flexural strengthening of the beam. In fact, the tensile stresses developed in CFRP sheet of the beam could not be effectively transferred to the column anymore. As a direct consequence, in the longitudinal CFRP laminates of the cross shape HCP, at the inferior face of the right beam, the tensile stresses increased significantly and one of these CFRP laminates ruptured. Therefore, the maximum bending capacity of the right beam during positive displacement (+106.4 kN·m at 2.67% drift) was reached by the rupture of this longitudinal CFRP laminate. In consequence of significant bond deterioration between this laminate and surrounding SHCC in the joint region, the flexural capacity of the left beam was also limited due to the sliding of this laminate during the lateral load reversal. This justifies the sudden drop in both positive and negative displacements at a drift level of 2.67%, as shown in Figure 8b.

The registered maximum bending moments for these specimens during both the positive and the negative loading displacements is also indicated in Table 2. Corresponding values for their virgin state and the percentage of the increase in their flexural capacity achieved after the retrofitting are also reported in this table. According to this data, the flexural capacity of the JPA0 after the retrofit increased up to 34.54% and 30.80%, for the negative and positive loading directions, respectively. The retrofitting system adopted in the JPC provided a larger increase in the resisting bending moments, since values of 74.8% and 47.5% are obtained for the negative and the positive loading, respectively. It should be noted that the values registered for the JPA0-R do not necessarily represent the flexural capacity of the beams, since the beam-column joint shear failure was the governing mode.

3.4. Drift Components

The lateral displacement of a beam-column joint can be decomposed into the contribution of the deformation developed in each of its elements. These drift components are the shear and the flexural deformations of both the columns and beams, fixed end rotations of the columns and the beams and eventually the distortion of the panel of the joint region in shear. In general, the shear deformation of the beams and columns has low contribution to the overall drift, as it is also the case of this study, and therefore can be neglected. Also the beams and columns flexural deformations may include the fixed end rotation since they were not independently measured. The flexural deformation of beams and columns is calculated using the average rotation of each slice determined by the measured values of the DTs installed on them. The contribution of the joint panel to the interstory drift is also calculated using the joint shear distortion. Measured values by the diagonally placed DTs are used to obtain the joint distortion at each level of interstory drift.

Figure 12 illustrates the contribution of each of the abovementioned components as the percentage of each level of the interstory drift during the steps of the positive displacements. The remaining portion of the graphs includes the shear deformation of the beams and columns, rigid body motion of the specimens due to the flexibility of supporting frames and finally local deformations at the supporting regions of the specimens.

According to the Figure 12a, the contribution of the beams flexural deformation in lateral displacement of JPA0-R increased up to 59% at the level of 1% drift. After this level of the drift the beams flexural contribution started decreasing, and reached to its minimum contribution of 19% at 4% drift. The joint distortion contribution started increasing after the drift level above 1.3% and at 3% drift has reached 35%, which was larger than the contribution of the other components. The maximum contribution of the joint distortion, 37%, has occurred at 3.33% of drift. The flexural contribution of the columns varied between 22% and 40%. Considering the observed damages and Figure 12a, it can be concluded that at 4% of drift the fixed end rotation of the column, due to the excessive sliding of the unbounded longitudinal reinforcements inside the joint region, and the joint shear distortion have dominated the interstory drift.

Figure 12b shows the contribution of the drift components in the interstory drift of JPC-R. It can be seen that the beams flexural contribution up to 1% of drift has increased up to 59%, similar to what was observed for JPA0-R. Between this drift level and 2.64% drift, the contribution of the beams flexural deformation was almost constant, but above 2.64% drifts the beams flexural contribution has increased and reached its maximum contribution of 86% at 4% of drift. Except at the drift level of 0.2%, where the contribution of the joint distortion was more than 20%, up to a drift level of 1% the joint distortion had almost a constant contribution with an average value of 12%. By increasing the imposed drift the contribution of the joint distortion has also increased and reached its maximum value of 23.8% at a drift level of 2.33%. Above this level of drift, the joint distortion had a reduction tendency so that at 4% of drift its contribution was only 5.2%. The column flexural contribution had a general tendency to decrease with the increase of the drift, with a 39% of contribution at a drift level of 0.2%, and 5.5% at the end of the test. This hierarchy of the contribution of each drift components for lateral displacement of JPC-R explains how the retrofitting system was efficient to decrease the joint shear distortion and, therefore, to maintain the columns undamaged.

3.5. Dissipated Energy

Energy dissipation and inelastic deformations of a lateral load resisting system indicate the potential of the structure to withstand the loading demands of seismic events. The amount of dissipated energy can be calculated from the enclosed area in each loading cycle as presented by the hysteresis response of lateral load *versus* lateral displacement. Integration of the dissipated energy with respect to the increment in lateral drift can result in total dissipated energy at each given level of interstory drift. The evolution of the dissipated energy for retrofitted and corresponding specimen in virgin state is presented in Figure 13. Both retrofitting solutions have provided an energy dissipation capacity higher than the one registered in the corresponding specimen in virgin state during all loading steps. In this respect, the retrofitting solution applied in JPC specimen was more effective. In fact, at 4% drift, the dissipated energy of JPA0-R was 52.3 kN·m, which is 23% larger than the energy dissipated in JPA0, while the JPC-R reached 54.03 kN·m corresponding to an increase of 84% comparing to dissipated energy of JPC.

3.6. Secant Stiffness

As a consequence of reversal and repeated actions of cyclic loading, the stiffness of a beam-column assembly can be deteriorated. To assess the stiffness degradation, the secant stiffness is estimated during the drift evolution, and its relationship is represented in Figure 14, for both the specimen in the retrofitted and virgin states. The secant stiffness is taken as the slope of the straight line which connects the peak loads at the positive and the negative displacements of the load *versus* displacement envelop at each level of the drift. According to this figure both specimens in the retrofitted state presented higher secant stiffness than in the virgin state, at least up to 3% drift. In terms of initial secant stiffness, JPA0-R presented the same stiffness as in its virgin state, while the initial secant stiffness of JPC-R was 22.5% higher than the value registered in its virgin state. This increase is attributed to the larger cross section after the retrofit, and higher level of concrete confinement introduced by the post-tension effect of the chemical anchors in all lateral faces of the framed elements. In addition, it should be mentioned that both retrofitting systems were able to recover (at least) the initial stiffness.

For the case of JPA0-R, when the first crack was formed, at 0.33% drift, the initial secant stiffness reduced more than 44%. Due to the concentration of damage at the superior face of the right beam of JPC-R, out of the retrofitted region, and initiation of the sliding of the longitudinal plain steel bars in this region, a significant drop in its secant stiffness at a drift level of 0.33% was registered. This stiffness reduction was about 58% of the initial secant stiffness.

3.7. Displacement Ductility

Ductility is the potential of a lateral load resisting system to undergo large inelastic deformations during its post-peak regime with only slight reduction in its ultimate lateral load carrying capacity. The ductility is generally quantified as a normalized displacement or a rotation index depending if the ductility is aimed to be assessed in terms of local or global behaviour, respectively. For the case of the present study, the displacement ductility index (μ_Δ) is calculated as the ratio of the ultimate lateral displacement (d_u) and the displacement at the yield point(d_y). The ultimate point can be defined as the displacement corresponding to a load level in the post-peak response of the specimen that is a fraction of the peak load (F_p). According to the available literature, this ratio can be taken between 10% and 20% [28-30]. The yield displacement can be obtained from a bi-linear curve assuming equivalent elastic-perfectly plastic response. To estimate this bi-linear curve, two conditions should be fulfilled: (i) the area under this curve should be equal to that for the envelope of load *versus* lateral displacement, and (ii) the deviation between these two curves, measured based on the absolute sum of the areas enclosed between these curves, should be the minimum (see Figure 15). The displacement ductility index is then calculated as the ratio between the ultimate displacement and the yield displacement. In this context it was assumed for the ultimate displacement the one corresponding to 10% loss of the peak load ($0.9F_p$). The envelope of the load *versus* drift and also the equivalent elastic-perfectly plastic curves estimated for both the retrofitted and virgin specimens are presented in Figure 16. Table 3 also indicates the yield and the ultimate displacement obtained for the calculation of the displacement ductility index for the positive and negative loading, where μ_Δ^V and μ_Δ^R are the ductility for the specimen in the virgin and retrofitted state, respectively. The reported ductility index is calculated as the average ductility using the corresponding values of displacement ductility in both positive and negative displacements. It is verified that for both retrofitted specimens the yield displacement has decreased when compared to the value registered in corresponding specimen in the virgin state. The reduction of the yield displacement is a consequence of the stiffness increase provided by the retrofitting system, with the main impact during the initial cycles. According to the results included in Table 3, the retrofitting strategy has assured an increase in terms of displacement ductility of 22.66% in the JPA0 specimen, while JPC-R presented a reduction of 18.2% in comparison to the displacement ductility factor registered in its virgin state. This reduction in ductility of JPC-R can be attributed to the loss of the right beam´s rotational ductility at the concentrated damage zone localized out of the retrofitted region, where the sliding of longitudinal steel bars at the superior face of the beam was initiated. Furthermore, due to the failure of

HCPs at the lateral face of the column, the CFRP sheet bonded to the critical section of the right beam lost its anchorage mechanism, which has promoted a gradient of tensile stress leading to the rupture of CFRP laminate at the inferior face of the HCP on the right beam.

Moreover, in comparison with JPA0-R, a lower damage in the joint region of JPC-R restricted the occurrence of any excessive joint shear distortion. Therefore, a reduction in displacement ductility of JPC-R is also defined by a lower contribution of the shear deformation at the joint region to the lateral displacement at the top of the column.

4. Conclusions

The effectiveness of a retrofitting system, based on attaching prefabricated HCPs to two severely damaged RC interior beam-column joints, was investigated by executing an experimental program with full-scale prototypes representative of RC frame-type buildings susceptible of severe damages if subjected to seismic events. HCP is a thin panel that conjugates the benefits of the ultra-high ductility of strain hardening cement composites (SHCC) with the high strength, elasticity modulus and durability of carbon fibre reinforced polymer (CFRP) reinforcement systems.

Both retrofitted specimens showed a superior performance in terms of hysteretic response, energy dissipation capacity, lateral load carrying capacity, beams flexural resistance and degradation of the secant stiffness than the corresponding values recorded when these specimens were tested in their virgin state.

While the adopted retrofitting system for JPA0-R resulted in higher displacement ductility with respect to its virgin state, a slight decrease in displacement ductility of JPC-R was registered. This is mainly associated to the increase in the initial stiffness, damage concentration out of the retrofitted region of the right beam and sliding of longitudinal steel bars at this region. Lower damage propagation in the joint region provided by the strengthening system and also partial detachment of the lateral HCPs during relatively early stages of cyclic loading are the complementary explanations for reduction in displacement ductility of JPC-R.

Progress in detachment of HCPs at the higher displacement demands was effectively restricted due to the presence of chemical anchors.

The much higher amount of dissipated energy presented by both the retrofitted specimens is attributed to the contribution of the HCPs by distributing the damage in the form of diffused multiple micro-cracks in the SHCC, increasing the concrete confinement of the joint, and offering resistance to the occurrence of a premature collapse due to the sliding of plain rebars.

Adding “L” shape HCPs to the retrofitting configuration resulted in lower shear stress development inside the joint region and, therefore, in lower damage in the joint region and its higher stability.

Acknowledgements

This work is supported by FCT (PTDC/ECM/114511/2009). The first author acknowledges the PhD scholarship SFRH/BD/65663/2009 provided by FCT. The authors also thank the collaboration of the following material suppliers: SIKA, Dow Chemical Co., ENDESA Compostilla Power Station, S&P Clever Reinforcement, and Hilti.

References

[1] Engindeniz M, Kahn LF, Zureick A-H. Repair and Strengthening of Reinforced Concrete Beam-Column Joints: State of the Art. ACI Struct J, 102(2) (2005), pp. 1-14

[2] Bousselham A. State of Research on Seismic Retrofit of RC Beam-Column Joints with Externally Bonded FRP. J Compos Constr, 14(1) (2010), pp. 49-61

[3] Tsonos AG. Effectiveness of CFRP-jackets and RC-jackets in post-earthquake and pre-earthquake retrofitting of beam–column subassemblages. Eng Struct, 30(3) (2008), pp. 777-793

[4] Tsonos A-DG. Performance enhancement of R/C building columns and beam–column joints through shotcrete jacketing. Eng Struct, 32(3) (2010), pp. 726-740

[5] Karayannis CG, Sirkelis GM. Strengthening and rehabilitation of RC beam–column joints using carbon-FRP jacketing and epoxy resin injection. Earthq Eng Struct Dyn, 37(5) (2008), pp. 769-790

[6] Al-Salloum Y, Almusallam T. Seismic Response of Interior RC Beam-Column Joints Upgraded with FRP Sheets. I: Experimental Study. J Compos Constr, 11(6) (2007), pp. 575-589

[7] Mukherjee A, Joshi M. FRPC reinforced concrete beam-column joints under cyclic excitation. Compos Struct, 70(2) (2005), pp. 185-199

[8] Pantelides CP, Okahashi Y, Reaveley LD. Seismic Rehabilitation of RC Frame Interior Beam-Column Joints with FRP Composites. In: The 14th World Conference on Earthquake Engineering. Beijing, China; 2008

[9] Esmaeeli E, Danesh F. Shear Strengthening of 3D Corner Beam-Column Connection Using Bidirectional GFRP Layers. In: Proceeding of Fourth International Conference on FRP Composites in Civil Engineering (CICE2008). Zurich; 2008

[10] Danesh F, Esmaeeli E, Alam MF. Shear Strengthening of 3D RC Beam-Column Connection Using GFRP: FEM Study. Asian J Appl Sci, 1(3) (2008), pp. 217-227

[11] Ha G-J, Cho C-G, Kang H-W, Feo L. Seismic improvement of RC beam–column joints using hexagonal CFRP bars combined with CFRP sheets. Compos Struct, 95(0) (2013), pp. 464-470

[12] Lee WT, Chiou YJ, Shih MH. Reinforced concrete beam–column joint strengthened with carbon fiber reinforced polymer. Compos Struct, 92(1) (2010), pp. 48-60

[13] Mahini SS, Ronagh HR. Strength and ductility of FRP web-bonded RC beams for the assessment of retrofitted beam–column joints. Compos Struct, 92(6) (2010), pp. 1325-1332

[14] Antonopoulos C, Triantafillou T. Experimental Investigation of FRP-Strengthened RC Beam-Column Joints. J Compos Constr, 7(1) (2003), pp. 39-49

[15] Engindeniz M, Kahn LF, Zureick A-H. Pre-1970 RC Corner Beam-Column-Slab Joints: Seismic Adequacy and Upgradability with CFRP Composites. In: The 14th World Conference on Earthquake Engineering. Beijing, China; 2008

[16] Eslami A, Ronagh H. Experimental Investigation of an Appropriate Anchorage System for Flange-Bonded Carbon Fiber–Reinforced Polymers in Retrofitted RC Beam–Column Joints. J Compos Constr, 18(4) (2014), pp.

[17] Benmokrane B, Mohamed HM. Durability Issues of FRP for Civil Infrastructure. In: 11th International Symposium on Fiber Reinforced Polymers for Reinforced Concrete Structures (FRPRCS11). Guimaraes; 2013

[18] Esmaeeli E, Manning E, Barros JA. Strain Hardening Fibre Reinforced Cement Composites for the Flexural Strengthening of Masonry Elements of Ancient Structures. Constr Build Mater, 38(special issue) (2013), pp. 1010-1021

[19] Esmaeeli E, Barros JAO, Baghi H. Hybrid Composite Plates (HCP) for Shear Strengthening of RC Beams. In: 11th International Symposium on Fiber Reinforced Polymers for Reinforced Concrete Structures (FRPRCS11). Guimaraes; 2013

[20] Barros JAO, Fortes AS. Flexural strengthening of concrete beams with CFRP laminates bonded into slits. Cem and Concr Compos, 27(4) (2005), pp. 471-480

[21] Fernandes CAL. Cyclic Behaviour of RC Elements with Plain Reinforcing Bars. PhD Thesis, Aveiro, Portugal: Civil Engineerig, Univeristy of Aveiro, 2012

[22] Fernandes C, Melo J, Varum H, Costa A. Cyclic Behavior of Substandard Reinforced Concrete Beam-Column Joints with Plain Bars. ACI Struct J, 110(1) (2013), pp. 137-147

[23] EN1992-1-1. Eurocode 2: Design of Concrete Structures. Part 1-1: General Rules and Rules for Buildings. Brussels, Belgium: European Committee for Standardization; 2004

[24] Park YJ, Ang AHS, Wen YK. Damage-Limiting Aseismic Design of Buildings. Earthq Spectr, 3(1) (1987), pp. 1-26

[25] Esmaeeli E, Barros JAO, Mastali M. Effects of curing conditions on crack bridging response of PVA reinforced cementitious matrix. In: 8th RILEM international symposium on fibre reinforced concrete: challenges and opportunities (BEFIB2012). Guimaraes, Portugal; 2012

[26] International Organization for Standardization – ISO 527-2:1996. Plastics — Determination of tensile properties — Part 2: Test conditions for moulding and extrusion plastics. London South Bank University

[27] Verderame GM, Fabbrocino G, Manfredi G. Seismic response of r.c. columns with smooth reinforcement. Part II: Cyclic tests. Eng Struct, 30(9) (2008), pp. 2289-2300

[28] Paulay T. Equilibrium criteria for reinforced concrete beam–column joints. ACI Struct J, 86(6) (1989), pp. 635-643

[29] EN 1998-3. 2005. Eurocode 8: Design of structures for earthquake resistance — Part 3: Assessment and retrofitting of buildings.

[30] Fardis M, Biskinis D. Deformation capacity of R.C. members, as controlled by flexure or shear. In: Performance-Based Engineering for Earthquake Resistant Reinforced Concrete Structures: A Volume Honoring Shunsuke Otani. University of Tokyo; 2003

Figures' captions

Figure 1: Details of adopted configurations for the interior beam-column joints.

Figure 2: Loading history adopted for the lateral displacement cycles (d_c^p: peak displacement for the corresponding cycle or set of cycles).

Figure 3: Test setup for the horizontally placed specimens [21]

Figure 4: The extent of damages before retrofitting (a) JPA0 and (b) JPC.

Figure 5: Details of the HCPs used for the repair of the damaged specimens (a) cross shape HCP for JPA0-R, (b) cross shape HCP for JPC-R, (c) section views of the cross shape HCPs, and (d) "L" shape HCP for JPC-R.

Figure 6: View of the repaired specimens (a) JPA0-R and (b) JPC-R.

Figure 7: Geometry of the slices assumed on each specimen to assess local deformations (the nodes are representing the regions where the displacement transducers were supported; dimensions in mm).

Figure 8: Hysteretic responses of the specimens (a) JPA0 and (b) JPC in the retrofitted and virgin states

Figure 9: Inclined cracks and bulging of the joint region of JPA0-R at the end of the test.

Figure 10: Damage distribution along the beam-column joint elements with close up views of micro-cracks at the end of testing of the JPC-R corresponding to (a) positive loading direction and (b) negative loading direction.

Figure 11: Development of the resisting bending moment at the interfaces of the beams with columns (the positive moment is assumed as the anticlockwise rotation) for specimen (a) JPA0-R and (b) JPC-R

Figure 12: Contribution of the beams flexure, the columns flexure, and the joint shear distortion to the overall drift of (a) JPA0-R, and (b) JPC-R

Figure 13: Evolution of the dissipated energy during the cyclic loading of (a) JPA0-R and JPA0, and (b) JPC-R and JPC.

Figure 14: Secant stiffness of (a) JPA0-R and JPA0, and (b) JPC-R and JPC.

Figure 15: Schematic representation of the definition of the equivalent bilinear curve for the evaluation of the displacement ductility index

Figure 16: Envelope of the load *versus* drift for both the retrofitted and virgin specimens along with the equivalent elastic-perfectly plastic curves of (a) JPA0-R and JPA0, and (b) JPC-R and JPC.

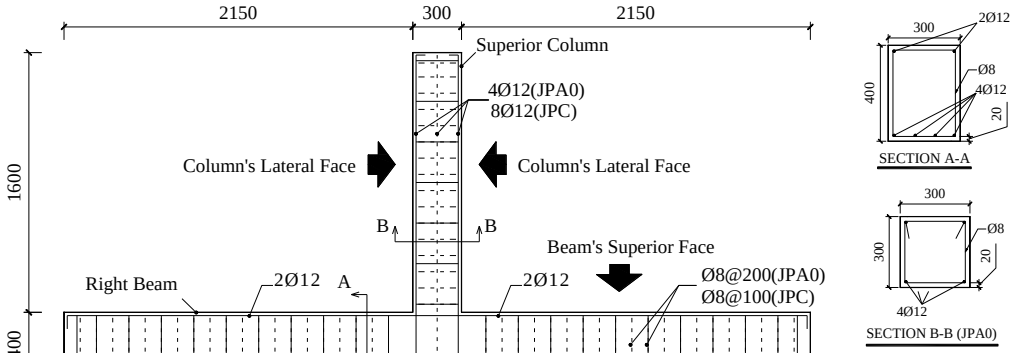

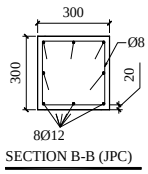

Figure 1: Details of adopted configurations for the interior beam-column joints.

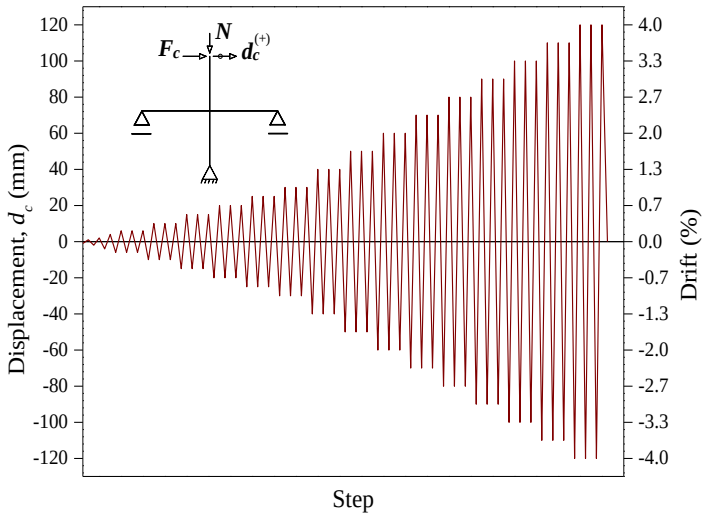

Cycle Numbers	d_c^p (mm)	Max drift (%)
1	±1	0.033
2	±2	0.067
3	±4	0.133
4 to 6	±6	0.20
7 to 9	±10	0.33
10 to 12	±15	0.50
13 to 15	±20	0.67
16 to 18	±25	0.83
19 to 21	±30	1.00
22 to 24	±40	1.33
25 to 27	±50	1.67
28 to 30	±60	2.00
31 to 33	±70	2.33
34 to 36	±80	2.67
37 to 39	±90	3.00
40 to 42	±100	3.33
43 to 45	±110	3.67
46 to 48	±120	4.00

Figure 2: Loading history adopted for the lateral displacement cycles (d_c^p: peak displacement for the corresponding cycle or set of cycles).

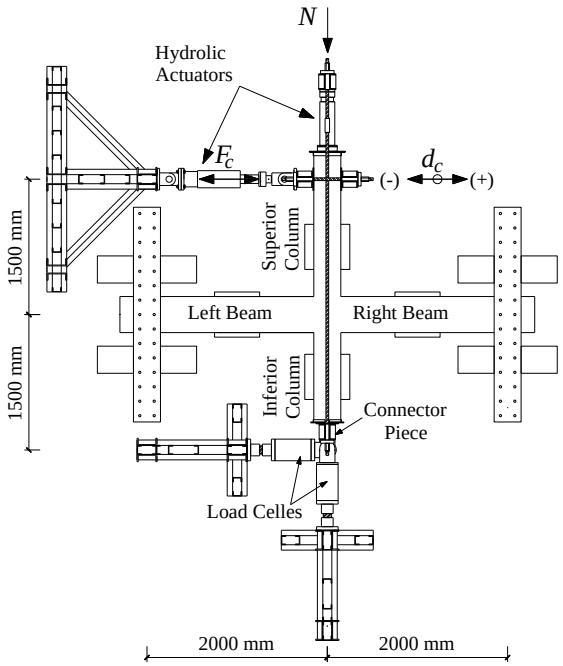

Figure 3: Test setup for the horizontally placed specimens [21]

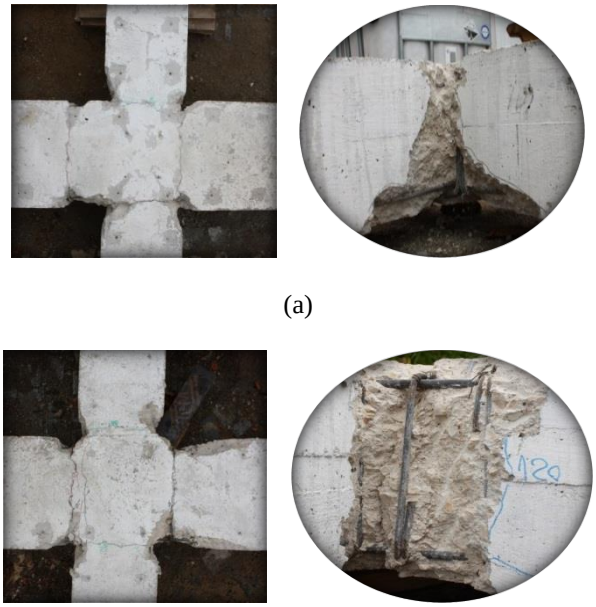

Figure 4: The extent of damages before retrofitting (a) JPA0 and (b) JPC.

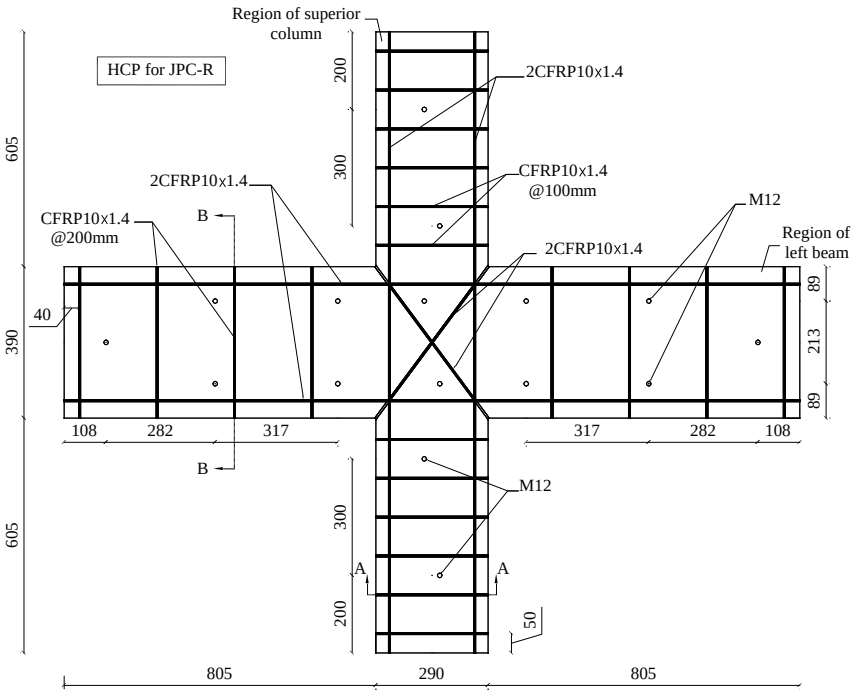
Region of superior column
HCP for JPC-R
2CFRP10x1.4
CFRP10x1.4 @100mm
M12
CFRP10x1.4 @200mm
Region of left beam
B
A
605
390
605
200
300
200
40
89
213
89
108
282
317
317
282
108
50
805
290
805

(a)

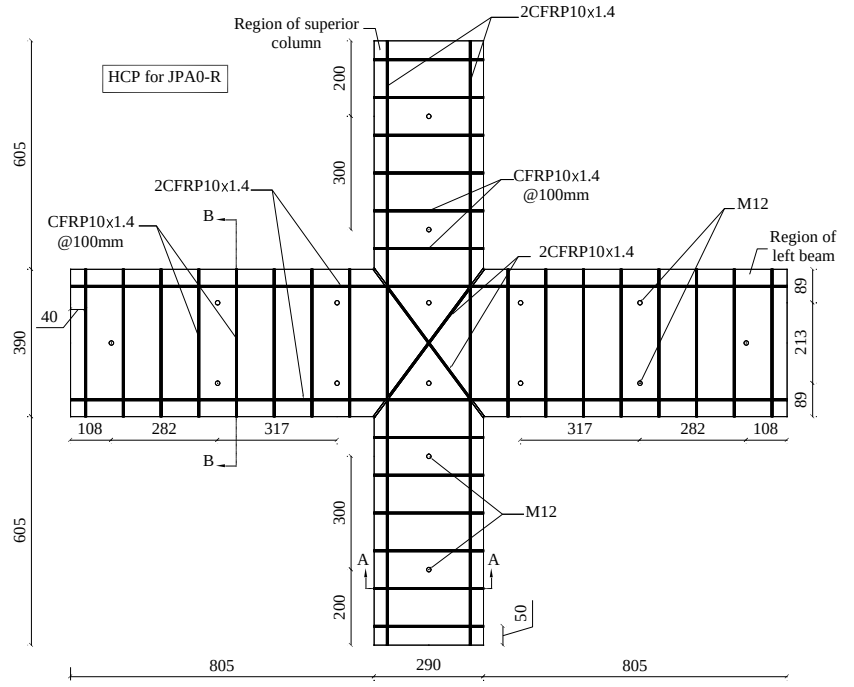
Region of superior column
HCP for JPA0-R
2CFRP10x1.4
CFRP10x1.4 @100mm
M12
CFRP10x1.4 @100mm
Region of left beam
B
A
605
390
605
200
300
200
40
89
213
89
108
282
317
317
282
108
50
805
290
805

(b)

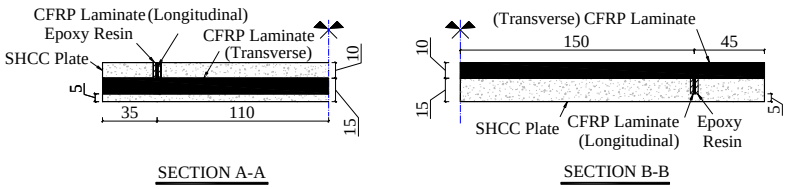

(c)

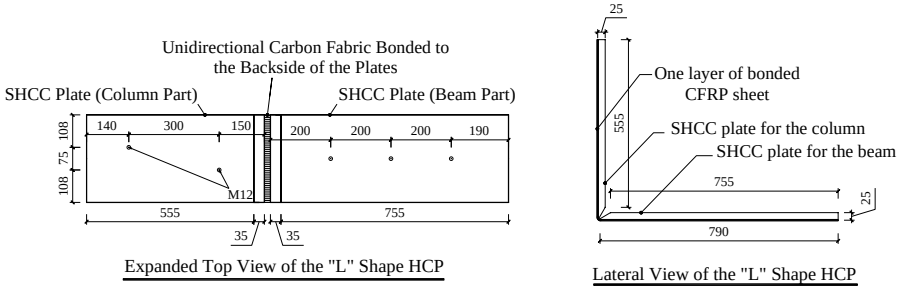

(d)

Figure 5: Details of the HCPs used for the repair of the damaged specimens (a) cross shape HCP for JPA0-R, (b) cross shape HCP for JPC-R, (c) section views of the cross shape HCPs, and (d) “L” shape HCP for JPC-R.

(a) (b)

Figure 6: View of the repaired specimens (a) JPA0-R and (b) JPC-R.

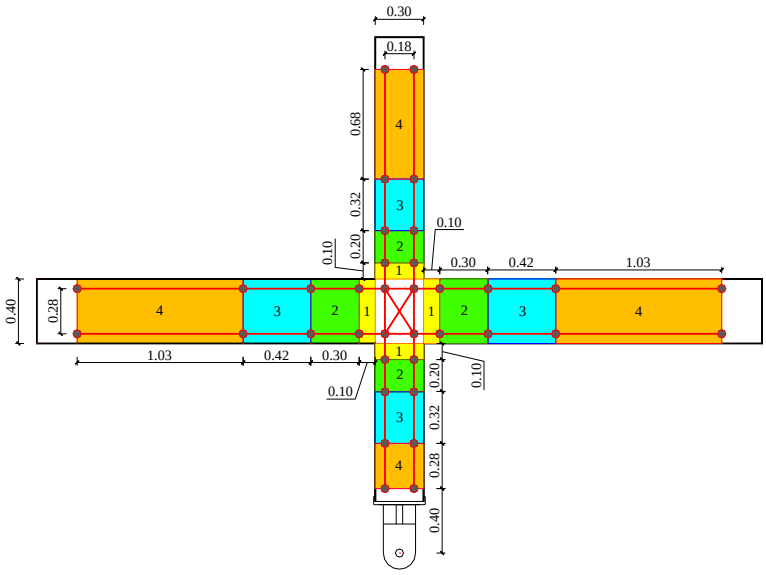

Figure 7: Geometry of the slices assumed on each specimen to assess local deformations (the nodes are representing the regions where the displacement transducers were supported; dimensions in mm).

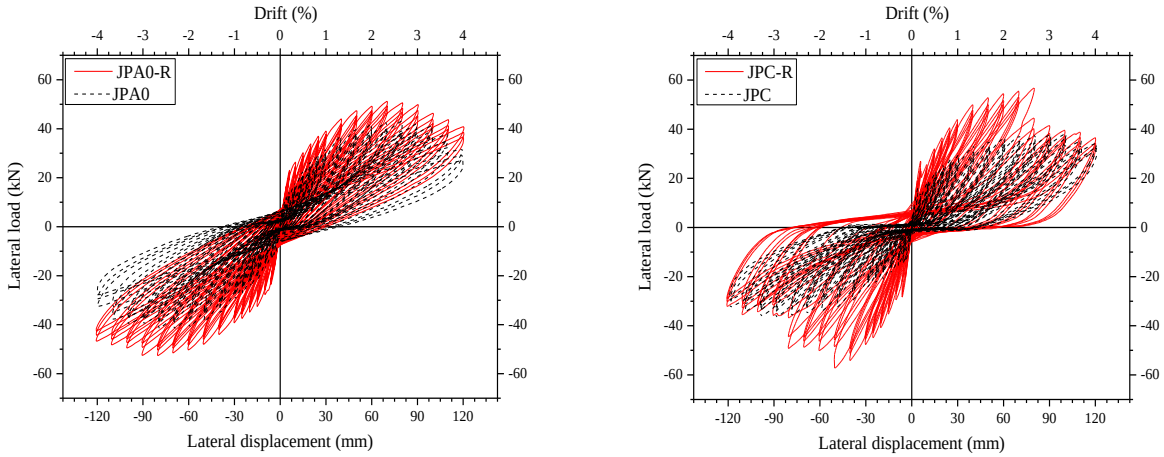

Figure 8: Hysteretic responses of the specimens (a) JPA0 and (b) JPC in the retrofitted and virgin states

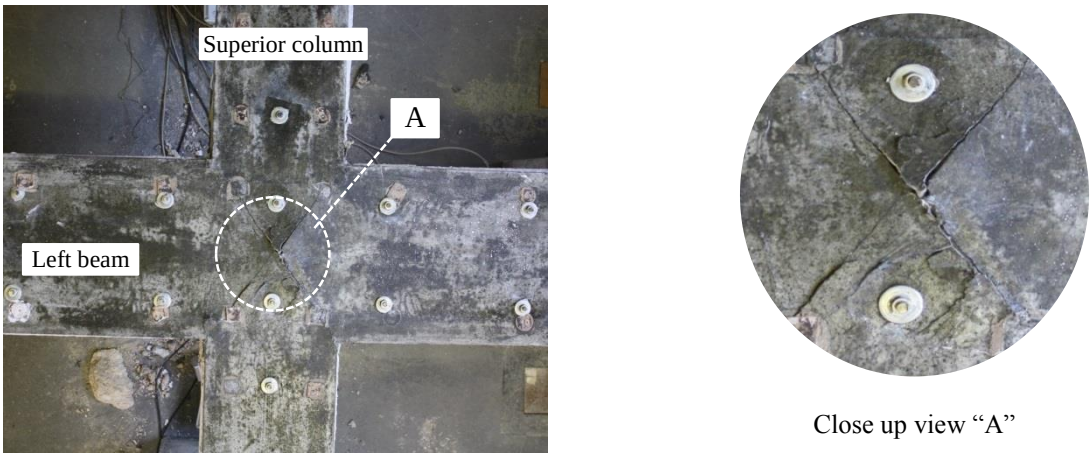

Figure 9: Inclined cracks and bulging of the joint region of JPA0-R at the end of the test.

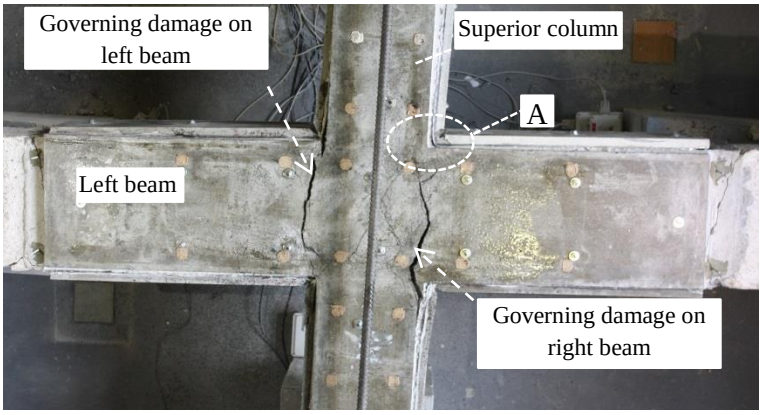

Close up view “A”

(a)

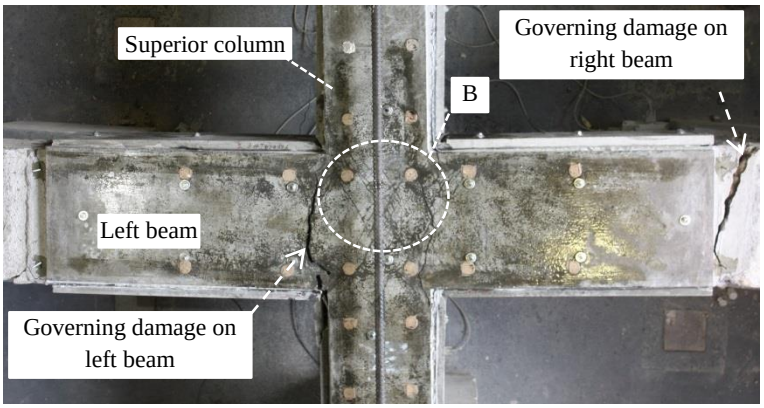

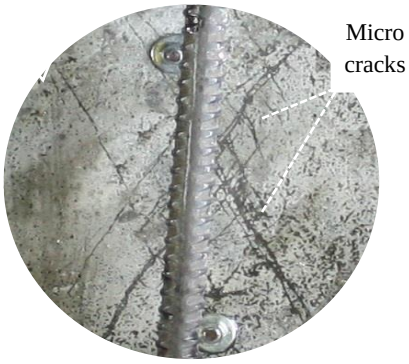

Close up view “B”

(b)

Figure 10: Damage distribution along the beam-column joint elements with close up views of micro-cracks at the end of testing of the JPC-R corresponding to (a) positive loading direction and (b) negative loading direction.

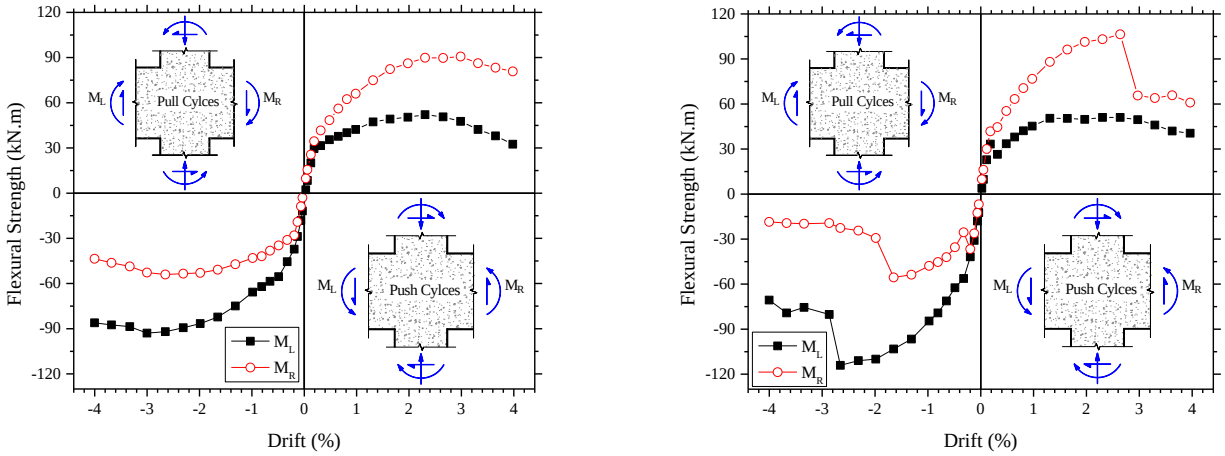

(a) (b)

Figure 11: Development of the resisting bending moment at the interfaces of the beams with columns (the positive moment is assumed as the anticlockwise rotation) for specimen (a) JPA0-R and (b) JPC-R

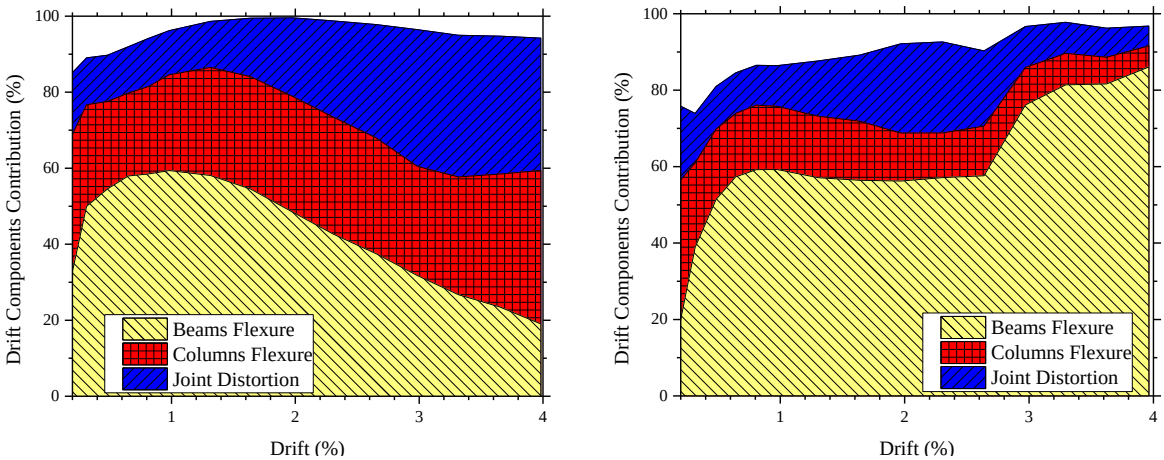

Figure 12: Contribution of the beams flexure, the columns flexure, and the joint shear distortion to the overall drift of (a) JPA0-R, and (b) JPC-R

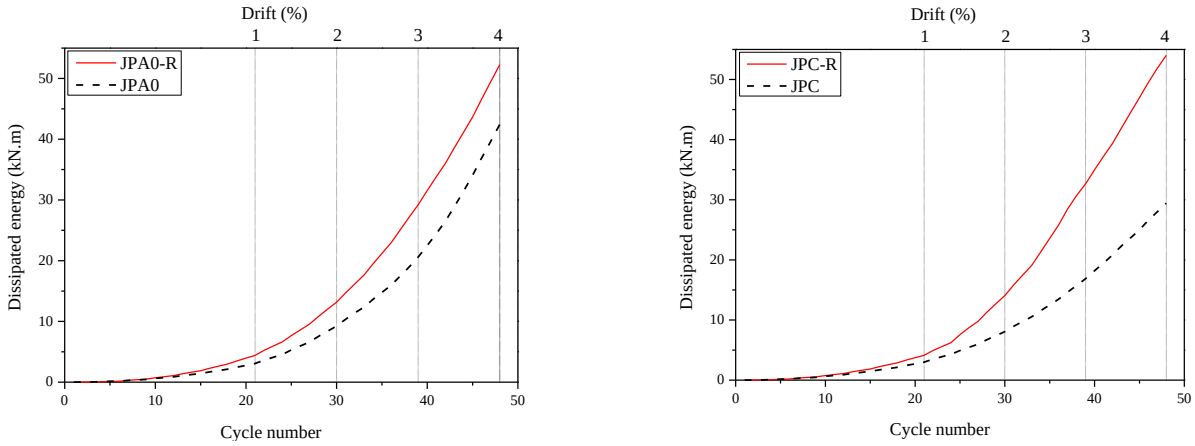

(a) (b)

Figure 13: Evolution of the dissipated energy during the cyclic loading of (a) JPA0-R and JPA0, and (b) JPC-R and JPC.

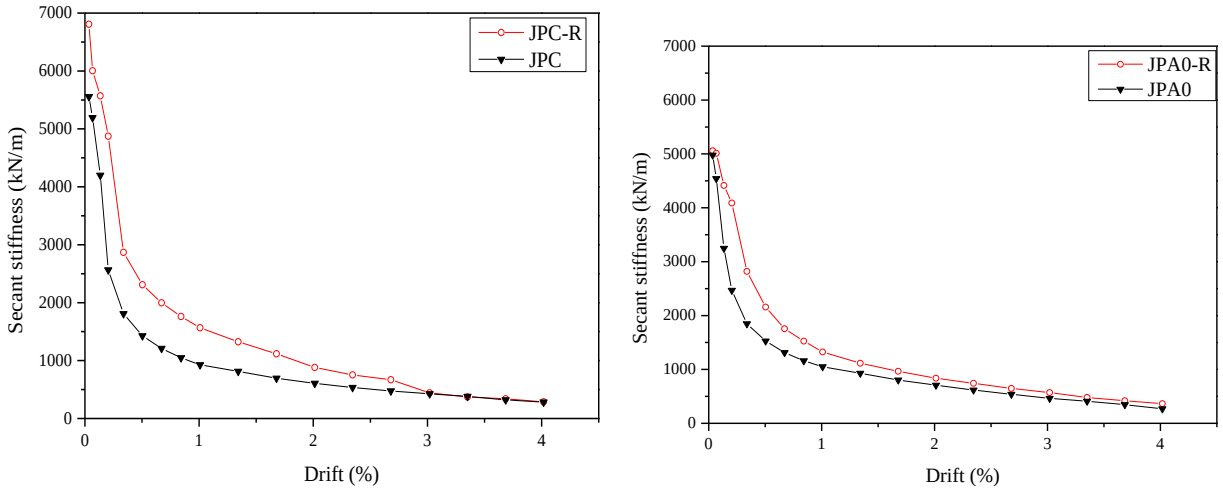

(a) (b)

Figure 14: Secant stiffness of (a) JPA0-R and JPA0, and (b) JPC-R and JPC.

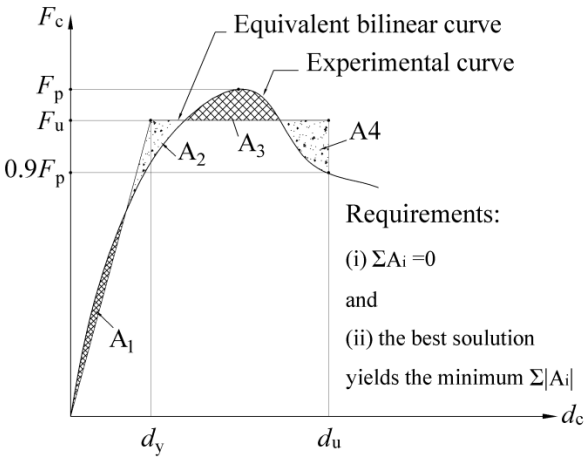

Figure 15: Schematic representation of the definition of the equivalent bilinear curve for the evaluation of the displacement ductility index

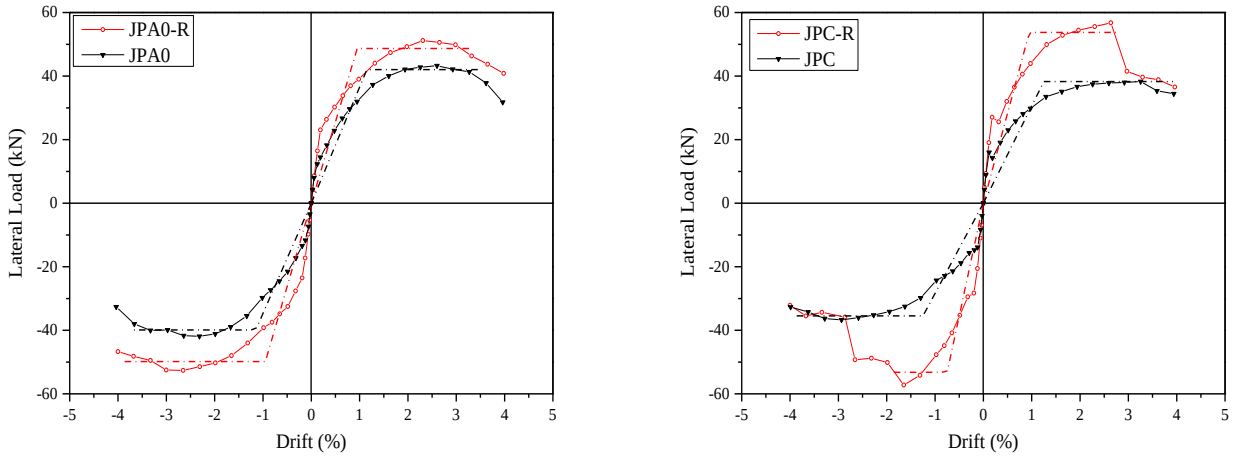

(a) (b)

Figure 16: Envelope of the load *versus* drift for both the retrofitted and virgin specimens along with the equivalent elastic-perfectly plastic curves of (a) JPA0-R and JPA0, and (b) JPC-R and JPC.

Tables' captions

Table 1: Maximum lateral load capacity and the corresponding drifts of the specimens in the retrofitted and virgin states

Table 2: Maximum bending moments developed in the beams of the retrofitted and the virgin specimens.

Table 3: Details of components for the evaluation of displacement ductility factor

Table 1: Maximum lateral load capacity and the corresponding drifts of the specimens in the retrofitted and virgin states

Specimen	Negative direction		Positive direction		Negative direction	Positive direction
	F_p^- (kN)	d_p^- (%)	F_p^+ (kN)	d_p^+ (%)	Increase in peak load	
JPA0-R	-52.6	-2.65	+51.2	+2.31	+25.5%	+18.2%
JPA0	-41.9	-2.31	+43.3	+2.60		
JPC-R	-57.2	-1.65	+56.8	+2.64	+54.5%	+48.3%
JPC	-36.7	-2.94	+38.3	+3.25		

Table 2: Maximum bending moments developed in the beams of the retrofitted and the virgin specimens.

Specimen	Negative direction		Positive direction		Negative direction		Positive direction	
	M_L (kN·m)	M_R (kN·m)	M_L (kN·m)	M_R (kN·m)	M_L increase (%)	M_R increase (kN·m)	M_L increase (kN·m)	M_R increase (kN·m)
JPA0-R	-92.95 (-3.00)*	-54.03 (-2.65)	+52.11 (+2.31)	+90.69 (+2.99)	22.5	34.5	30.8	13.4
JPA0	-75.85 (-2.32)	-40.16 (-2.32)	+39.84 (+2.59)	+79.95 (+2.59)				
JPC-R	-114.13 (-2.66)	-55.58 (-1.65)	+51.09 (+2.64)	+106.4 (+2.64)	61.3	74.8	47.5	45.1
JPC	-70.75 (-3.28)	-31.79 (-2.94)	+34.64 (+1.94)	+73.34 (+3.25)				

** Values in parentheses indicate the corresponding drift in percentage at maximum bending moment.*

Table 3: Details of components for the evaluation of displacement ductility factor

Specimen	Negative direction		Positive direction		μ_Δ	$\frac{\mu_\Delta^R - \mu_\Delta^V}{\mu_\Delta^V}$ (%)
	d_y^- (mm)	d_u^- (mm)	d_y^+ (mm)	d_u^+ (mm)		

JPA0-R	-28.5 (-0.95)*	-116 (-3.86)	+28.6 (+0.95)	+100.5 (+3.35)	3.8	22.6%
JPA0	-34.5 (-1.15)	-110.5 (-3. 68)	+34.5 (+1.15)	+105.2 (+3.51)	3.1	
JPC-R	-22.5 (-0.75)	-57.6 (-1.92)	+28.5 (+0.95)	+82.9 (+2.76)	2.7	-18.2%
JPC	-37.5 (-1.25)	-117.3 (-3.91)	+37.5 (+1.25)	+117.7 (+3.92)	3.3	

** Values in parentheses indicate the corresponding drift in percentage at maximum bending moment.*